Stretchable Supercapacitor with Adjustable Volumetric Capacitance Based on 3D Interdigital Electrodes

Fengwang Li, Jitao Chen, Xusheng Wang, Mianqi Xue,* and G. F. Chen*

Reduced graphene oxide (rGO)-based materials have shown good performance as electrodes in flexible energy storage devices owing to their physical properties, high specific surface area, and excellent electrical conductivity. Here, a novel road is reported for fabricating high-performance supercapacitors based on 3D rGO electrodes and solid electrolyte multilayers via pressure spray printing and machine coating. These supercapacitors demonstrate high and adjustable volumetric capacitance, excellent flexibility, and stretchability. The results show that this commercial strategy has its essential merits such as low-cost, inexpensive, and simple fabrication for large area production. These properties are in the favor of fabricating high-performance supercapacitor to meet the practical energy demands in devices, especially flexible electronic devices. Furthermore, this novel 3D interdigital electrode concept can be widely applied to other energy devices for enhancing performances and to other micro devices for reducing cost.

1. Introduction

The recent development of carbon-based flexible supercapacitors ignites tremendous interest in the realization of the next-generation energy storage devices with high capacitance density, good operational safety, ultralong cycling life as well as low cost and environmental friendliness.[1–3] In fact, although supercapacitors have been extensively studied for several decades with carbon materials as electrodes,[4] till the experimental realization of the first reduced graphene oxide (rGO)-based supercapacitor,[5] has it become the increasing interest of numerous research groups in both academic and industry around the world for the practical application in energy storage.[6–13] rGO, with the advantages of good electrical conductivity, low mass density, very high specific surface area, and being easy to fabricate,[14] has shown good performance as electrodes in energy harvesting/storage devices, such as solar cells,[15–17] secondary batteries,[18] and especially supercapacitors.[8,10–12] Combined with the solution preparation and the flexibility, rGO has already been expected as a competitive alternative for the next-generation flexible supercapacitors.

Despite being one kind of the ideal electrode materials, the present rGO-based materials are restricted by unsatisfactory volumetric capacitance in flexible devices. On the one hand, the specific capacitance of rGO is not high (generally 50–200 F g^{-1}), which depends on the electrical double layer at the interface between electrode and electrolyte.[19] On the other hand, the large inert space in practical devices (large volume ratio of encapsulation layers in the device) also accounts for the low volumetric energy density.[9] These two points have plagued the integration of rGO-based flexible supercapacitors into roll-up displays, wearable device or other flexible microdevices. Therefore, researchers are striving to find new feasible method for preparing rGO-based electrodes with satisfactory electrochemical performance, including high volumetric capacitance and long cycle life. Previously, we fabricated flexible microsupercapacitor with well-ordered conducting polymer nanostructures on rGO interdigital electrodes to enhance the specific capacitance through synergistic effect.[20] This high-performance microsupercapacitor provides a promising power source whose reliability and performance might meet the energy demands of the next-generation miniaturized electronic devices, especially flexible devices. More recently, some feasible methods have also been studied by other research groups. For example, 3D interpenetrating graphene electrodes have been fabricated by electrochemical reduction of GO for ultrahigh rate supercapacitors;[21] Gao co-workers proposed a coaxial wet-spinning assembly approach to continuously spin polyelectrolyte-wrapped graphene/CNT core-sheath yarns and the yarn-based supercapacitors showed a capacitance of 177 mF cm^{-2} in solid electrolyte (SE);[22] carbon microfibers made of aligned single-walled carbon nanotubes (SWCNTs) and nitrogen-doped rGO sheets are produced and show a specific volumetric capacity of 300 F cm^{-3} in polyvinyl alcohol (PVA)/H_3PO_4 electrolyte;[23] to further improve the capacitance, metal oxides, and conducting polymer are introduced to composite with carbon materials.[24,25]

These modifications show valuable characteristics in enhancing the performance, especially the specific capacitance;

F. Li,[+] Prof. M. Xue, Prof. G. F. Chen
Institute of Physics and Beijing National Laboratory for Condensed Matter Physics
Chinese Academy of Sciences
Beijing 100190, China
E-mail: xuemq@iphy.ac.cn
Prof. J. Chen, X. Wang
Beijing National Laboratory for Molecular Sciences
College of Chemistry and Molecular Engineering
Peking University
Beijing 100871, P. R. China
E-mail: chenjitao@pku.edu.cn
[+]Present address: School of Chemistry, Monash University, Clayton, Victoria 3800, Australia

DOI: 10.1002/adfm.201500718

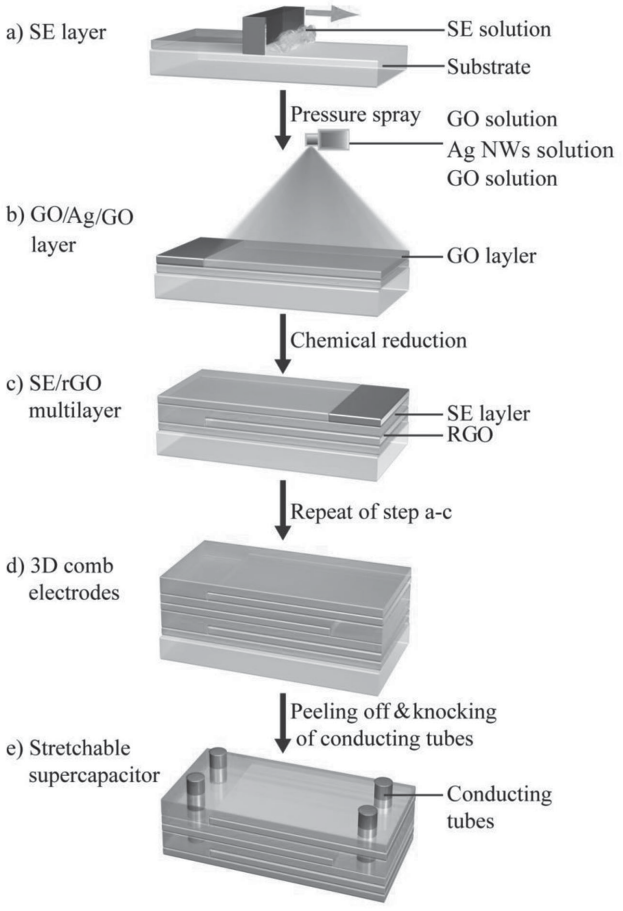

Figure 1. Schematic illustration of the in situ fabrication of SRARS-based stretchable supercapacitor. a) Machine coating PVA film on the PP substrate. b) Press spraying GO/Ag-NWs/GO thin film on the surface of one-end protected PVA film. c,d) Repeating the previous two steps to get stretchable 3D interdigital electrodes. e) Machine knocking conducting tubes into two ends of supercapacitors.

however, it still remains a great challenge to find a feasible way to industrialize rGO-based flexible devices while maintaining high performance. Herein, we propose a novel and simple idea, which contains two industrial paths: machine coating and pressure spray printing for fabricating supercapacitors with 3D interdigital electrodes. Each interdigital electrode contains a layer of SE film consisted of PVA and H_3PO_4 by means of machine coating and a sandwich layer of rGO thin film (contains two rGO thin layer as active material with a layer of Ag nanowires (Ag-NWs) as current collector, also described as rGO/Ag-NWs/rGO) through pressure spray printing. By introducing the novel concept of 3D interdigital electrode, the volumetric capacitance can be controlled and raised to a higher level which is no longer limited by the excess inert space in conventional double-layer designed device. On the other hand, the all-solid-state design endows the supercapacitor flexibility and stretchability, which improves the safety of the final devices (without flammable electrolyte) and adaptability to external load circuit. Therefore, all these merits of this strategy reveal this supercapacitor as a possibility in high-capacity energy storage.

2. Results and Discussion

Figure 1 schematically illustrates the procedure used for fabricating SE/rGO multilayers, which is based on machine coating and pressure spray. First, pre-prepared H_3PO_4–PVA gel was coated on the upper surface of a polypropylene (PP) film, and plasticized via heating in an oven in high humidity. GO solution, Ag-NWs solution and GO solution were sprayed on the surface of one-end protected (as shown in Figure 1b) PVA film in sequence, and then chemically reduced by hydrazine vapor. The transform of GO to rGO is conformed from Raman spectrum and X-ray photoelectron spectroscopy (XPS) spectrum (Supporting Information). Second, another PVA film was coated on the surface of as-fabricated PVA-rGO layer without any protection, subsequently another GO/Ag-NWs/GO film was sprayed on the surface with the-other-end-protection (as shown in Figure 1c). Highly stretchable 3D interdigital-electrode-based supercapacitors were formed after repeating the previous two steps to get desired layer. Both the ends of supercapacitors (half-GO-layers part) were folded and then a couple of conducting tubes were knocked in for electrical measurements. In this paper, GO was prepared via the modified Hummers method as previously described.[20,26,27] The PVA layer plays the role of both electrolyte and separator while the rGO film acts as electrodes. Both the rGO film and Ag-NWs layer performs as current collectors.

In this typical procedure, after the machine coating process, the as-fabricated 10 μm thickness PVA gel was cured in high humidity (75%) to control the surface roughness of the SE surface. The GO was dispersed into the mixture of water and

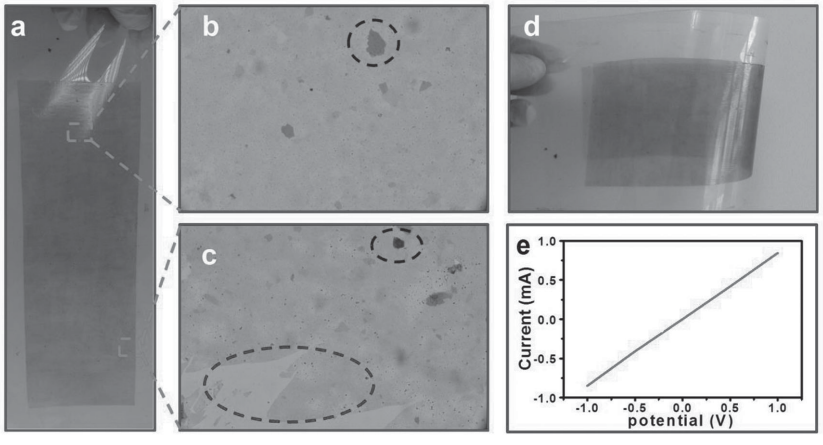

Figure 2. Morphology of SE/rGO film. a) Optical image of a two-layer SE/rGO film on a PP substrate. b) Optical magnified view of SE/rGO film. Inset ellipse: the aggregation of rGO during the solution process. c) Optical image of the edge of SE/rGO film. Upper inset ellipse: the aggregation of rGO. Lower inset ellipse: defects on the edge of SE/rGO film. d) Optical image shows the flexibility of as-fabricated SE/rGO films on a PP substrate. e) The conductivity of rGO layer (without Ag-NWs layer) on SE film.

ethanol (2:8 volume ratio) for rapid drying. Single layer of GO film was sprayed dozens of times for the full coverage. Each sprayed liquid film on the surface should be as thin as possible (just be a membrane) to avoid the deformation of thin film. The thickness of each SE and rGO film can be easily controlled by adjusting the concentration of precursor solution and the spraying parameters. **Figure 2**a demonstrates the optical image of the first two layers of SE and rGO thin film on PP substrate which presents a gray translucent appearance. Large-area, centimeter-long rGO layer assembled well on SE film. The color of rGO film becomes darker when increasing the spraying number. There are some dark color dots in the optical images, which result from the aggregation of rGO during the solution process (Figure 2b,c). Also, at the edges of the rGO film, there are defects caused by edge effect, which is shown in the ellipses on Figure 2c. Figure 2d presents the flexibility of SE/rGO film on PP substrate. As shown in the Figure 2e, the obtained rGO patterns are electrically continuous, exhibiting ohmic behavior. The large resistance (around kΩ cm^{-1} scale) is probably due to the defects of the rGO sheets, the scattering effects arising from the stacking of rGO and the residual oxygen-containing groups.[20] It was characterized that the conductivity of the rGO thin film varied about 5% under bending and even folding conditions shown in the Figure 2d, and the reduction of conductivity is less than 10% even under elongation ratio (ε) at 1.4. It is attributed to the interformational sliding of multilayer rGO.

A set of images in **Figure 3** exhibits the morphologies of SE/rGO thin film. Atomic force microscopy (AFM) image (Figure 3a) and scanning electron microscopy (SEM) image (Figure 3b) show the continuous surface of rGO with some wrinkles. After hydrazine-vapor reduction, the resulted rGO patterns display similarities in film morphology and thickness to the original GO patterns. Figure 3c shows the cracking of jagged edge under ε at 1.8 and the multilayers of rGO in single thin film. To improve the electrical collecting efficiency, Ag-NWs were introduced as collectors. Figure 3d illustrates the Ag-NWs with the diameter around 60 nm. Figure 3e shows the side view of sprayed Ag-NWs layer on the surface of rGO layer, exhibiting fine cross stacking. The resistance of Ag-NWs thin film is less than 30 Ω $\square^{-1}$, which is smaller than that of the rGO film alone. It was also characterized that the conductivity of the Ag-NWs thin film varied about 3% under bending and even folding conditions. The superior conductivity of Ag-NWs in these conditions renders them as good collectors. The platform and cross-section morphology of SE/rGO/Ag-NWs/rGO/SE (SRARS) film are displayed in Figure 3e,f, respectively. The magnifying view of the cross-section of SRARS layer clearly shows the interface between SE layer and rGO layer (Figure 3h). The following electrochemical test demonstrate that the performance of as-prepared SRARS supercapacitors remains almost unchanged when stretching under a strain of 130%, even under the stretching process. It enlightens a broad application in stretchable energy storage devices to meet the increasing demand of portable and wearable multifunctional electronic devices.

We investigated the electrochemical properties of SRARS supercapacitor by cyclic voltammetry (CV) and galvanostatic charge–discharge measurements. As shown in **Figure 4**a, the CV curves of the ten-layer SRARS supercapacitor (unless

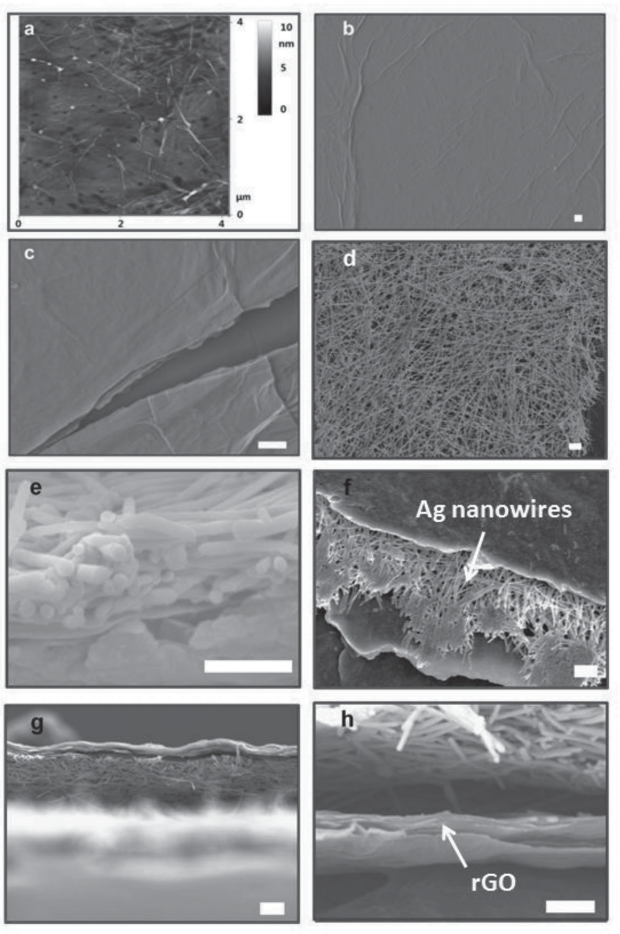

Figure 3. Microstructures of SE/rGO film. a) AFM image of the rGO layer on SE film. b) SEM image of the rGO layer on SE film. c) Vertical view of the fracture morphology of rGO film. d) SEM image of Ag-NWs with the diameter around 60 nm. e) The side view of sprayed Ag-NWs layer on the surface of rGO layer. f) The platform of SE/rGO/Ag-NWs/rGO/SE film. g) The view of the cross-section of SE/rGO/Ag-NWs/rGO film. h) Magnifying view of the cross-section of SE/rGO/Ag NWs/rGO layer. Scale bar: b–d,f,g) 1 μm; e,h) 500 nm.

specific note, we use ten-layer supercapacitor for the following tests) show a nearly symmetrical rectangular shape at a series of scan rate (from 20 to 500 mV s^{-1}) and this good rectangular shape even retained at a high scan rate of 500 mV s^{-1}, which indicates the good electrochemical performance of the SRARS supercapacitor.[28] Figure 4b depicts the galvanostatic charge–discharge curve of SRARS supercapacitor between 0 and 1.0 V at the current density of 0.5 A g^{-1}. The curves are close to triangular shape, confirming the formation of a typical electric double-layer capacitor (EDLC).[4] From the galvanostatic charge–discharge curve, the specific capacitances of ten-layer SRARS supercapacitor is calculated according to the following equation

$$C_m = It/m\Delta V$$

where C_m is the specific capacitance (F g^{-1}), ΔV is 1 V, I is the charge/discharge current, t is charge or discharge time, and m

is the weight of electrode materials. In this supercapacitor, the specific capacitances are 121 F g^{-1}.

To meet with the demands in wearable device or other flexible microdevices, a power source should be flexible and work in different stretching conditions at different operation power. We have studied the electrochemical behaviors of our supercapacitors while strain is applied to demonstrate the feasibility of the stretchable supercapacitors. The specific capacitances with different ε at current density of 0.5 A g^{-1} are illustrated in Figure 4c. The specific capacitance is 119.5 F g^{-1} for ε at 1.18, remaining 98.8% compared with the specific for ε at 1.0. Although the specific surface area of electrodes is affected by stretching, the specific capacitance does remain unchanged obviously. The two-layer SRARS supercapacitor with ε at 1.0 and 1.3 is shown via optical images, respectively (inset of Figure 4c; the appearance of ten-layer supercapacitor is almost black and is difficult to compare via optical images). Region 1 in the rectangular marquee is the folded end of supercapacitor and it contains a column of knocked-in conducting tubes (as staples). The side part marked as Region 2 displays greater transparency than the central part of the supercapacitor when under the horizontal tension; this is attributed to half amount of rGO layers at both sides in the spray process. The electrochemical performance of SRARS supercapacitor was further evaluated under bending at 180°. The CV curve shows negligible shape change (Figure S2, Supporting Information) and the galvanostatic charge–discharge curve of the supercapacitor under bending of 180° at a current density of 0.5 A g^{-1} in Figure 4d almost overlap completely with the unbending one. Both the stretching and bending tests demonstrate the high flexibility of the SRARS supercapacitor, which is highly desirable for flexible electronics.

Figure 5 shows the stability of SRARS supercapacitor. The specific capacitance of the SRARS electrode is 140.2 F g^{-1} at a discharge current of 0.01 A g^{-1}, while it retains about 80.7% with increasing of current density from 0.01 to 10 A g^{-1} (Figure 5a). It is worth to point out that the specific capacitance of the SRARS electrode can retains more than 93% with increasing of current densities from 1 to 10 A g^{-1}. Meanwhile, the specific capacitance values of the ten-layer SRARS supercapacitor changes slightly under different ε and different charge/discharge current densities, even as high as 10 A g^{-1}. These results suggest that SRARS electrodes have good stretchability and rate capability. The cycling stability of the ten-layer SRARS supercapacitor is illustrated by specific capacitance (calculated from galvanostatic charge–discharge curves) with a constant current density of 0.5 A g^{-1} up to 4000 cycles. Figure 5b shows the cycle stability of these all-solid-state devices with different ε at 1.0 and 1.3. The discharge capacitance loss after 4000 consecutive cycles is negligible, at about 3%, no matter ε is 1.0 or 1.3. Furthermore, the capacitance at a current density of 1.0 A g^{-1} retains more than 99% of its initial capacitance after bending for more than 1000 times at 180° (Figure 4c). The superior stability of the SRARS supercapacitor is attributed to the intrinsic EDLC property of this supercapacitor, in which the electrical charge is stored in the double layer.[4] The outstanding feature of EDLCs is their reversibility for that electrostatic interaction is infinitesimally detrimental to electrodes and solution stability and EDLC can be charged–discharged thousands of times.

In the practical application, it is more meaningful to use the volumetric energy density of the whole supercapacitor to evaluate the energy storage performance of a microdevice, rather than the gravimetric energy density based on active electrode materials.[23] The capacitance of the SRARS supercapacitor can be easily controlled by adjusting the number of electrode layers. The specific capacitance of the SRARS supercapacitor changes slightly with different layer number (Figure S3, Supporting Information), which makes it feasible to increase the specific volumetric capacitance of the whole device by simply increasing the number of SRARS (as shown in Figure 5c, the data are values normalized to the whole device volume, not the volume of active rGO electrodes). While the rGO thickness is 250 nm, the volumetric capacitance of our system is around 6 F cm^{-3}, and further reaches to 28.3 F cm^{-3} with the rGO thickness increasing to 1 μm. The volumetric capacitance of our system possesses a superior level to normal commercial supercapacitors (1–100 F cm^{-3}),[29,30] and pre-eminently in carbon-based flexible supercapacitor (Table S1, Supporting Information). It should point out that the volumetric capacitance could reach 77.9 F cm^{-3} with the 5 μm rGO layer which is, to the best of our knowledge, almost the highest value of the carbon-based supercapacitance. Nevertheless, the using of

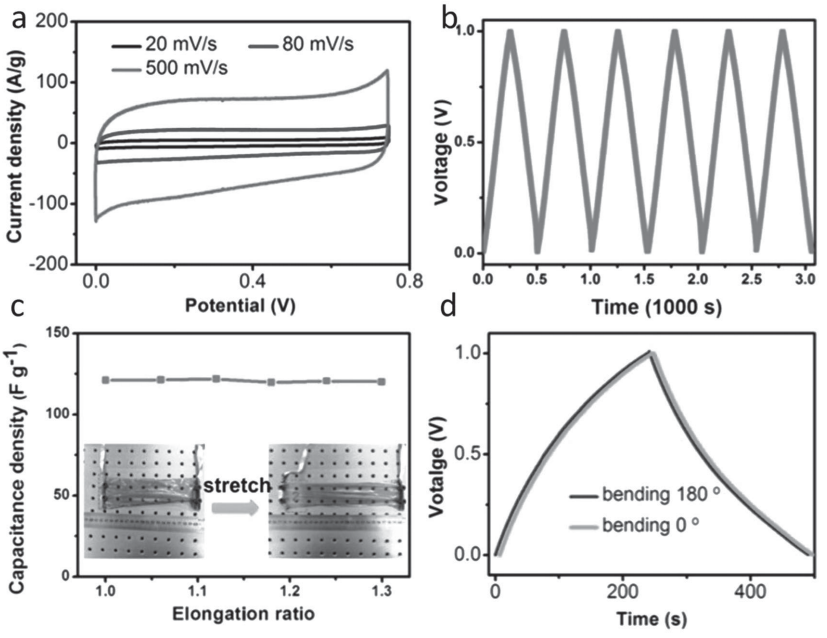

Figure 4. Electrical characterizations of SRARS supercapacitor. a) CV curves of the supercapacitor at different scan rate. b) Galvanostatic charge–discharge curves of the supercapacitor at current density of 0.5 A g^{-1} after calculating the relative value. c) Changes of capacitance density with different ε at current density of 0.5 A g^{-1}. Inset: optical images of as-fabricated two-layer SRARS film with ε at 1.0 and 1.3, respectively. d) Galvanostatic charge–discharge curves of the supercapacitor at different bending angles.

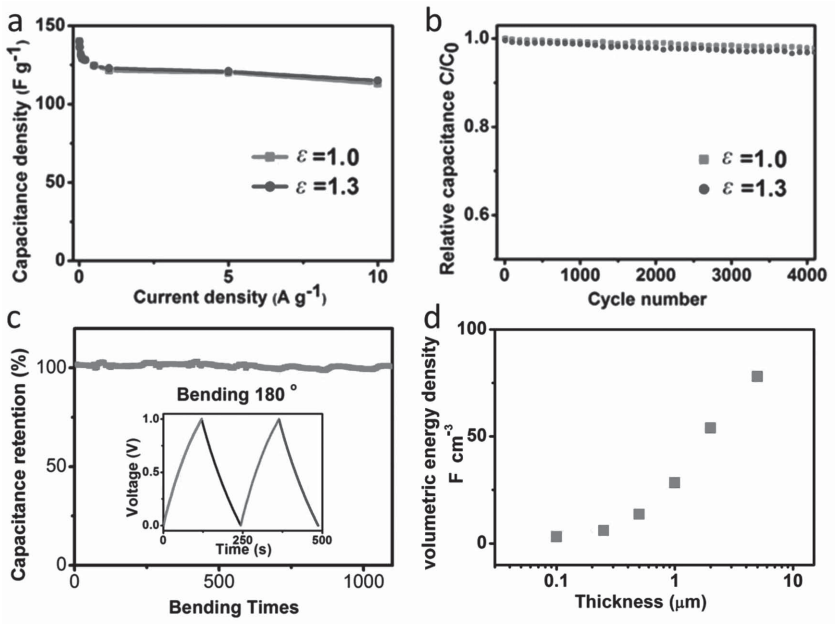

Figure 5. Stability of SRARS supercapacitor. a) Specific capacitance of SRARS supercapacitor with different ε at 1.0 (red) and 1.3 (blue) at different charge–discharge current densities. b) Cycle stability of the all-solid-state devices at 0.5 A g^{-1} with different ε at 1.0 (red) and 1.3 (blue). The high voltage of the test is 1 V. c) Stability at bending conditions. Inset: the first two galvanostatic charge–discharge cycles of the supercapacitor at current density of 1.0 A g^{-1} under bending conditions. d) Specific volumetric capacitance at different thickness of rGO film.

5 μm thick rGO affected the stretchability of the supercapacitor to some extent. Although graphene is a good candidate as supercapacitor electrode material for their ultrahigh surface area and excellent conductivity, the volumetric performances are usually poor. A possible explanation lies in the strong π–π interaction between layers, which seriously restrict the ion accessibility.[31] However, in our case, we utilized a simple way to construct a stack of layered rGO electrode to achieve a high volumetric performance. It may result from two aspects: first, each rGO electrode is comprised of only a few layers of rGO, which decreases the severe stacking and improves the ion accessibility;[32] second, the stack of rGO electrode in one single device could make full use of the device space, reducing the volume ratio of encapsulation layers in the device.

With a useful but simple design, micro-/interdigital electrode is widely used in micro devices for the space-saving, and also has been used for increasing the specific capacitance of supercapacitors.[13,20,28] Here, we propose a modified novel 3D interdigital electrode structures (as shown in **Figure 6**) to enhance the performance of supercapacitors in order to meet the practical demands and simplify the fabrication technique to facilitate the industrial production. All the procedures were carried out by low-cost industrial equipment with very simple steps, which was demonstrated in the previous text. The using of rGO in our method ensures high capacitance and stability of the supercapacitor. Meanwhile, rGO and SE are in favor for flexible electronics as they avoid the risk of harmful liquid leakage. The performance of our supercapacitor, as a flexible device (easily rolled-up) is demonstrated in Figure S4 (Supporting Information). A prototype of a supercapacitor film was fabricated and then rolled up. Three light-emitting diodes (LED, the working potential is 1.5 V) were successfully lit with high brightness. Along with the flexibility and stretchability of this all-solid-state polymer-based device, these supercapacitors can match the demanding applications as the power system in flexible electronics.

3. Conclusion

To conclude, we succeeded in finding a novel way to fabricate rGO-based all-solid-state stretchable supercapacitors with 3D interdigital electrodes to achieve high volumetric capacitance. The capacitance of the supercapacitor can be easily adjusted by changing the number of SRARS layers. Through the overlaying of plenty ultrathin SE and rGO film in the *z*-axis, it can maximize space utilization while maintaining the specific capacitance high enough. The successful realization of such supercapacitors suggests that it is possible to make a high power/energy density energy storage device in a simple but safety way. The high volumetric energy/power density ensures the possibility to integrate these flexible supercapacitors into specific applications as power system, such as roll-up displays, wearable device or other flexible microdevices.

4. Experimental Section

All materials and chemicals were purchased commercially and used as received. All the chemical reagents were purchased from Sinopharm Chemical Reagent Beijing Co. except where noted. XPS measurements were performed using an ESCALab220i-XL electron spectrometer from VG Scientific using 300 W Al Kα radiation. Raman measurements were performed with a Renishaw Invia Raman Microscope spectrometer. The conductance measurements were recorded by Keithley 2400 sourcemeter. SEM images were recorded with JEOL 4600 and 7401 microscope. AFM image was recorded with dimension 3100. Optical images were recorded with Nikon TE2000. All electrochemical measurements were conducted with a computer-controlled CHI660B electrochemical analyzer (Shanghai Chenhua Instrument Corporation, China).

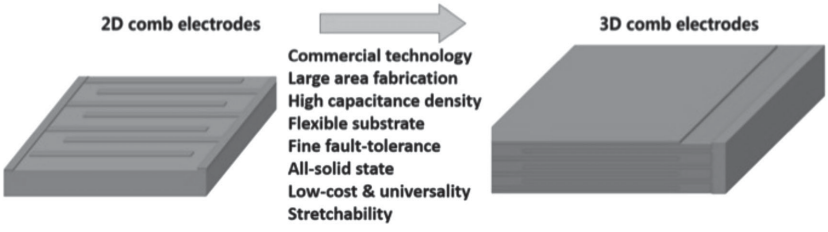

Figure 6. Schematic illustration of the novel design of 3D interdigital electrodes.

Fabrication of GO and Silver Nanowire Solutions: GO was prepared by the oxidation of natural graphite powder (325 mesh, Qingdao Huatai Lubricant Sealing S&T Co. Ltd., Qingdao, China) according to a modified Hummers' method reported in our previous literatures.[20,26,27] The GO aqueous solution was prepared by dispersing as-prepared GO sheets in water after sonication. GO was first sonicated in mild sonication for 2 h to get stable aqueous suspension. Then a strong sonication was applied to the presonicated GO solution for 20 min to break big GO sheets. The resulting GO solution was then separated in two steps: first centrifuged at 1500 rpm for 2 h and the top layer solution was collected in order to remove most of the large GO sheets, and then centrifuged at 10 000 rpm for 2 h to remove the small GO sheets with diameter less than 300 nm. The bottom part of the GO solution was collected and used for electrode fabrication. Silver nanowires were synthesized according to a reported procedure.[33] A mixture of 1 g of polyvinylpyrrolidone (PVP, purchased from Beijing Yili Fine Chemical Co., Ltd.) and 30 mL of ethylene glycol was heated and stabilized at 170 °C in a flask. Then 0.07 g of AgCl was added to the flask slowly. After 10 min, 0.310 g of $AgNO_3$ was added to the sample dropwise and then kept for 30 min. After the final centrifuge as reported procedure,[33] the precipitate of Ag NWs is dispersed in 10 mL of ethanol.

Fabrication of 3D Interdigital Electrode: The gel electrolyte was prepared by mixing PVA powder ($M_w \approx 10\,000$, Aldrich) with water (mass fraction, 10%) and then 0.8 g concentrated H_3PO_4. As-fabricated gel was predried at 40 °C, and then was coated on the upper surface of the PP film with 10 μm thickness. The GO solution, Ag-NWs solution and GO solution were sprayed on the surface of one-end protected PVA film in sequence to form GO/Ag-NWs/GO film, and then was chemically reduced with hydrazine vapor.[34] In this procedure, it is worth mentioning that the manipulation should be careful to avoid the deformation of thin film. Another PVA film was coated on the surface of as-fabricated PVA-rGO layer without any protection, and subsequently another GO/Ag-NWs/GO film was sprayed on the surface with the-other-end protection. Both the ends of supercapacitors were folded and then a few conducting tubes were knocked in after repeating the two steps mentioned before.

Electrochemical Measurements: All electrochemical measurements were carried out at room temperature. The CV and galvanostatic charge–discharge measurements were used to accurately evaluate the electrochemical performance of the devices. Different current densities were applied and a current density of ≈0.5 A g^{-1} was used for the cycling life tests.

Supporting Information

Supporting Information is available from the Wiley Online Library or from the author.

Acknowledgements

The authors wish to thank R. Li and Y. Zhu for their fruitful discussions. This work was supported by the Natural Science Foundation of China (Grant No. 21304002), Qinghai Province Science and Technology program (Grant Nos. 2012-G-Y28 and 2013-G-Q12A-1) and Shenzhen Science and Technology Innovation Commission (Grant No. JCYJ20120829170028561).

Received: February 22, 2015
Published online: June 15, 2015

[1] a) X. Yang, C. Cheng, Y. Wang, L. Qiu, D. Li, *Science* **2013**, *341*, 534; b) M.-Q. Zhao, C. E. Ren, Z. Ling, M. R. Lukatskaya, C. Zhang, K. L. Van Aken, M. W. Barsoum, Y. Gogotsi, *Adv. Mater.* **2015**, *27*, 339.
[2] a) R. Ruoff, *Nature* **2012**, *483*, S42; b)A. K. Geim, *Nature* **2012**, *490*, 192; c) J. Yan, Q. Wang, T. Wei, Z. Fan, *Adv. Energy Mater.* **2014**, *4*, 1300816.
[3] a) T. Chen, R. Hao, H. Peng, L. Dai, *Angew. Chem. Int. Ed.* **2015**, *54*, 618; b) Z. Zhang, J. Deng, X. Li, Z. Yang, S. He, X. Chen, G. Guan, J. Ren, H. Peng, *Adv. Mater.* **2015**, *27*, 356; c) X. Chen, H. Lin, J. Deng, Y. Zhang, X. Sun, P. Chen, X. Fang, Z. Zhang, G. Guan, H. Peng, *Adv. Mater.* **2014**, *26*, 8126; d) Y. Zhang, W. Bai, X. Cheng, J. Ren, W. Weng, P. Chen, H. Peng, *Angew. Chem. Int. Ed.* **2014**, *53*, 14564; e) H. Sun, X. You, G. Guan, X. Fang, J. Deng, P. Chen, H. Peng, *Angew. Chem. Int. Ed.* **2014**, *53*, 9526; f) X. Chen, H. Lin, P. Chen, G. Guan, Y. Luo, H. Peng, *Adv. Mater.* **2014**, *26*, 4444; g) Z. Yang, J. Deng, X. Chen, J. Ren, H. Peng, *Angew. Chem. Int. Ed.* **2013**, *52*, 13453.
[4] L. L. Zhang, X. S. Zhao, *Chem. Soc. Rev.* **2009**, *38*, 2520.
[5] L.Song, A. Zhamu, J. Guo, B. Z. Jang, *US Patent 7623340 B1*, **2006**.
[6] X. Huang, Z. Yin, S. Wu, X. Qi, Q. He, Q. Zhang, Q. Yan, F. Boey, H. Zhang, *Small* **2011**, *7*, 187.
[7] K. S. Kim, Y. Zhao, H. Jang, S. Y. Lee, J. M. Kim, K. S. Kim, J.-H. Ahn, P. Kim, J.-Y. Choi, B. H. Hong, *Nature* **2009**, *457*, 706.
[8] L. L. Zhang, X. Zhao, M. D. Stoller, Y. Zhu, H. Ji, S. Murali, Y. Wu, S. Perales, B. Clevenger, R. S. Ruoff, *Nano Lett.* **2012**, *12*, 1806.
[9] J. J. Yoo, K. Balakrishnan, J. Huang, V. Meunier, B. G. Sumpter, A. Srivastava, M. Conway, A. L. M. Reddy, J. Yu, R. Vajtai, P. M. Ajayan, *Nano Lett.* **2011**, *11*, 1423.
[10] Y. Cheng, S. Lu, H. Zhang, C. V. Varanasi, J. Liu, *Nano Lett.* **2012**, *12*, 4206.
[11] Z. Niu, J. Chen, H. H. Hng, J. Ma, X. Chen, *Adv. Mater.* **2012**, *24*, 4144.
[12] M. Beidaghi, C. Wang, *Adv. Funct. Mater.* **2012**, *22*, 4501.
[13] M. Xue, Z. Xie, L. Zhang, X. Ma, X. Wu, Y. Guo, W. Song, Z. Li, T. Cao, *Nanoscale* **2011**, *3*, 2703.
[14] C. N. R. Rao, A. K. Sood, K. S. Subrahmanyam, A. Govindaraj, *Angew. Chem. Int. Ed.* **2009**, *48*, 7752.
[15] J. M. Yun, J. S. Yeo, J. Kim, H.-G. Jeong, D.-Y. Kim, Y.-J. Noh, S.-S. Kim, B.-C. Ku, S.-I. Na, *Adv. Mater.* **2011**, *23*, 4923.
[16] F. Bonaccorso, Z. Sun, T. Hasan, A. C. Ferrari, *Nat. Photonics* **2010**, *4*, 611.
[17] S. W. Tong, N. Mishra, C. L. Su, V. Nalla, W. Wu, W. Ji, J. Zhang, Y. Chan, K. P. Loh, *Adv. Funct. Mater.* **2013**, *24*, 1904.
[18] Y. Zhu, S. Murali, W. Cai, X. Li, J. W. Suk, J. R. Potts, R. S. Ruoff, *Adv. Mater.* **2010**, *22*, 3906.
[19] M. D. Stoller, S. Park, Y. Zhu, J. An, R. S. Ruoff, *Nano Lett.* **2008**, *8*, 3498.
[20] M. Xue, F. Li, J. Zhu, H. Song, M. Zhang, T. Cao, *Adv. Funct. Mater.* **2012**, *22*, 1284.
[21] K. Sheng, Y. Sun, C. Li, W. Yuan, G. Shi, *Sci. Rep.* **2012**, *2*, 247.
[22] L. Kou, T. Huang, B. Zheng, Y. Han, X. Zhao, K. Gopalsamy, H. Sun, C. Gao, *Nat. Commun.* **2014**, *5*, 3754.
[23] D. Yu, K. Goh, H. Wang, L. Wei, W. Jiang, Q. Zhang, L. Dai, Y. Chen, *Nat. Nanotechnol.* **2014**, *9*, 555.
[24] J. Lee, M. Shin, S. Kim, H. Cho, G. Spinks, G. Wallace, M. Lima, X. Lepro, M. Kozlov, R. Baughman, S. Kim, *Nat. Commun.* **2013**, *4*, 1970.
[25] J. Tao, N. Liu, W. Ma, L. Ding, L. Li, J. Su, Y. Gao, *Sci. Rep.* **2013**, *3*, 2286.
[26] H. Liu, J. Gao, M. Xue, N. Zhu, M. Zhang, T. Cao, *Langmuir* **2009**, *25*, 12006.
[27] F. Li, M. Xue, X. Ma, M. Zhang, T. Cao, *Anal. Chem.* **2011**, *83*, 6426.
[28] Y. S. Moon, D. Kim, G. Lee, S. Y. Hong, K. K. Kim, S. M. Park, J. S. Ha, *Carbon* **2015**, *81*, 29.
[29] P. Simon, A. Burke, *Interface* **2008**, *17*, 38.
[30] S. Zhang, N. Pan, *Adv. Energy Mater.* **2015**, *5*, 1401401.
[31] Y. Zhu, L. Li, C. Zhang, G. Casillas, Z. Sun, Z. Yan, G. Ruan, Z. Peng, A. O. Raji, C. Kittrell, R. H. Hauge, J. M. Tour, *Nat. Commun.* **2012**, *3*, 1225.
[32] X. Yang, C. Cheng, Y. Wang, L. Qiu, D. Li, *Science* **2013**, *341*, 534.
[33] L. B. Hu, H. S. Kim, J. Y. Lee, P. Peumans, Y. Cui, *ACS Nano* **2010**, *4*, 2955.
[34] Q. He, H. G. Sudibya, Z. Yin, S. Wu, H. Li, F. Boey, W. Huang, P. Chen, H. Zhang, *ACS Nano* **2010**, *4*, 3201.